Efficient Dye-Sensitized Solar Cells with Catalytic Multiwall Carbon Nanotube Counter Electrodes

Won Jae Lee,* Easwaramoorthi Ramasamy, Dong Yoon Lee, and Jae Sung Song

Energy Conversion Devices Research Center, Korea Electrotechnology Research Institute, Changwon 641-120, Korea

ABSTRACT We report the successful application of multiwall carbon nanotubes (CNTs) as electrocatalysts for triiodide reduction in a dye-sensitized solar cell (DSSC). Defect-rich edge planes of bamboolike-structure multiwall CNTs facilitate the electron-transfer kinetics at the counter electrode−electrolyte interface, resulting in low charge-transfer resistance and an improved fill factor. In combination with a dye-sensitized TiO_2 photoanode and an organic liquid electrolyte, a multiwall CNT counter-electrode DSSC shows 7.7% energy conversion efficiency under 1 sun illumination (100 mW/cm^2, air mass 1.5 G). The short-term stability test at moderate conditions confirms the robustness of CNT counter-electrode DSSCs.

KEYWORDS: carbon nanotube • charge-transfer resistance • dye-sensitized solar cell • counter electrode • efficiency

1. INTRODUCTION

Dye-sensitized solar cells (DSSCs) have been intensively studied as prospective alternative to conventional solar cells, largely because of its simple fabrication process, high energy conversion efficiency, and low-cost materials (1, 2). Unlike inorganic p−n junction solar cells, in DSSCs light absorption and charge carrier transport take place in different phases. A porous network of nanosize TiO_2 particles serves as a charge-transport medium on which a monolayer of dye molecules is chemically adsorbed. Upon illumination, electrons are injected from the photoexcited dye into the conduction band of TiO_2, while holes shuttle toward the counter electrode through a iodide/triiodide (I^-/I_3^-) redox electrolyte. After this process is performed, the electron reaches the counter electrode and reduces the I_3^- ion and the electrical circuit is completed (3). The counter electrode is generally prepared by depositing a thin layer of platinum catalyst on a fluorine-doped tin oxide (FTO) conducting glass substrate followed by heat treatment at 400 °C (4). Although the required platinum loading for optimum performance of the solar cell is small, the dissolution of the platinum film in the corrosive electrolyte and high-temperature heat treatment necessitate the development of stable and cost-effective counter-electrode materials (5−7). The latter property also restricts the choice of flexible substrates. In this respect, different forms of carbon material have been studied as a cost-effective and stable catalyst for I_3^- reduction reaction in DSSCs (8−12).

Carbon nanotubes (CNTs) are unique nanoscale objects with the combined advantages of large surface area, high electrical conductivity, and chemical stability. CNTs can be classified into two main categories: single-wall CNTs and multiwall CNTs. A single-wall CNT consists of a single rolled-up graphene sheet, whereas a multiwall CNT consists of several coaxially arranged graphene sheets. Multiwall CNTs are often produced in a hollow structure, where the graphene sheet is parallel with the tube axis, or bamboolike structure, where graphene sheets are formed at an angle to the tube axis (13). Because the edge planes of the graphene exhibit faster electron-transfer kinetics than the basal planes, single-wall and hollow-structure multiwall CNTs (which are made up of nearly perfect atomically smooth basal planes) may not be suitable for favorable electrocatalytic applications (14, 15). In this letter, we report the successful application of bamboolike-structure multiwall CNT counter electrodes for I_3^- reduction in DSSCs. Defect-rich edge planes of bamboolike-structure CNTs facilitate the electron-transfer kinetics, and therefore the device (Figure 1) shows an energy conversion efficiency comparable to that of conventional platinum counter-electrode DSSCs.

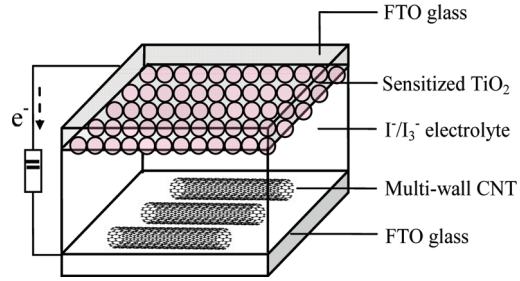

FIGURE 1. Schematic of a multiwall CNT counter-electrode DSSC. The device is illuminated from the TiO_2 photoanode side.

2. EXPERIMENTAL SECTION

Preparation of CNT Electrodes. CNT electrodes were prepared using a paste that contains multiwall CNTs, an organic binder, and distilled water. In brief, 0.16 g of (carboxymethyl)-cellulose (CMC) sodium salt (Sigma Aldrich, viscosity 400−800

* E-mail: wjlee@keri.re.kr.
Received for review December 19, 2008 and accepted May 5, 2009
DOI: 10.1021/am800249k

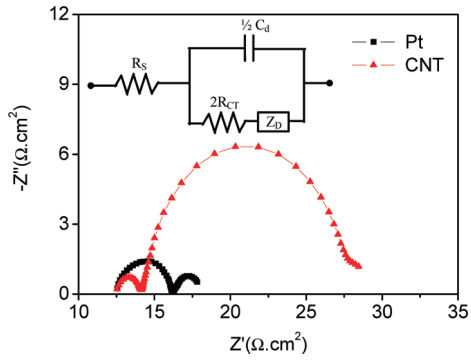

FIGURE 2. Nyquist plot of a thin-layer symmetric cell and its corresponding equivalent circuit. The triangle shows the performance of multiwall CNT electrodes, whereas the square represents the screen-printed platinum electrodes.

cP) was dissolved in 19.84 mL of distilled water (Samchun Pure Chemical Co., Kyungki-do, Korea). A total of 2.25 g of multiwall CNTs (Carbon Nanotech Inc., Korea; ~20 nm diameter, 5 μm length) was then added to the binder solution and ball-milled for 1 h at 100 rpm. The resulting homogeneous CNT slurry was tape-cast onto a previously cleaned FTO glass substrate (Hartford Glass Co., Newington, CT; sheet resistance 15 Ω/□) followed by drying at 50 °C for 10 h in air. For a good comparison with multiwall CNT electrodes, conventional platinum electrodes were also prepared by depositing a commercially available platinum paste (Solaronix, platinum catalyst T/SP) on a FTO glass substrate, which was subsequently heat treated at 400 °C for 30 min in air. A thin-layer symmetric cell was fabricated by stacking two identical multiwall CNT or platinum electrodes on each other with a 80-μm-thick Surlyn polymer foil spacer and sealed in a hot press. The interelectrode space was filled with a liquid electrolyte consisting of LiI (0.5 mol/L), I_2 (0.05 mol/L), and 4-*tert*-butylpyridine (0.5 mol/L) in acetonitrile.

Solar Cell Fabrication. The working electrode for DSSC was prepared by depositing the TiO_2 paste (Solaronix, titanium nanoxide HT/SP) on an FTO glass substrate (Hartford Glass Co., Newington, CT; sheet resistance 15 Ω/□) and sintered at 500 °C for 1 h. After cooling to 80 °C, sintered electrodes were immersed in a 0.3 mM solution of *cis*-bis(isothiocyanato)bis(2,2′-bipyridyl-4,4′-dicarboxylato)ruthenium(II) bis(tetrabutylammonium) dye (Solaronix, N719) in ethanol for 24 h. Sensitized TiO_2 electrodes were rinsed with anhydrous ethanol, dried in nitrogen gas, and assembled with CNT or platinum counter electrodes. An organic liquid electrolyte with a composition of LiI (0.5 mol/L), I_2 (0.05 mol/L), and 4-*tert*-butylpyridine (0.5 mol/L) in acetonitrile was introduced into the cell via vacuum backfilling through an injection hole on the counter-electrode side. Finally, the electrolyte injection hole was sealed with Surlyn and a microscope cover glass.

Electrochemical and Photovoltaic Characterization. Electrochemical impedance spectroscopy measurements were carried out with a computer-controlled potentiostat (Princeton Applied Research, Parstat 2273) in the frequency range of 0.1 Hz to 100 kHz. The magnitude of the alternative signal was set to 10 mV. Current−voltage characteristics of the DSSCs were performed both in the dark and at a range of air mass 1.5 G illumination intensity using an Oriel (model 91160) solar simulator and a Keithley 2400 source meter. The intensity of incident

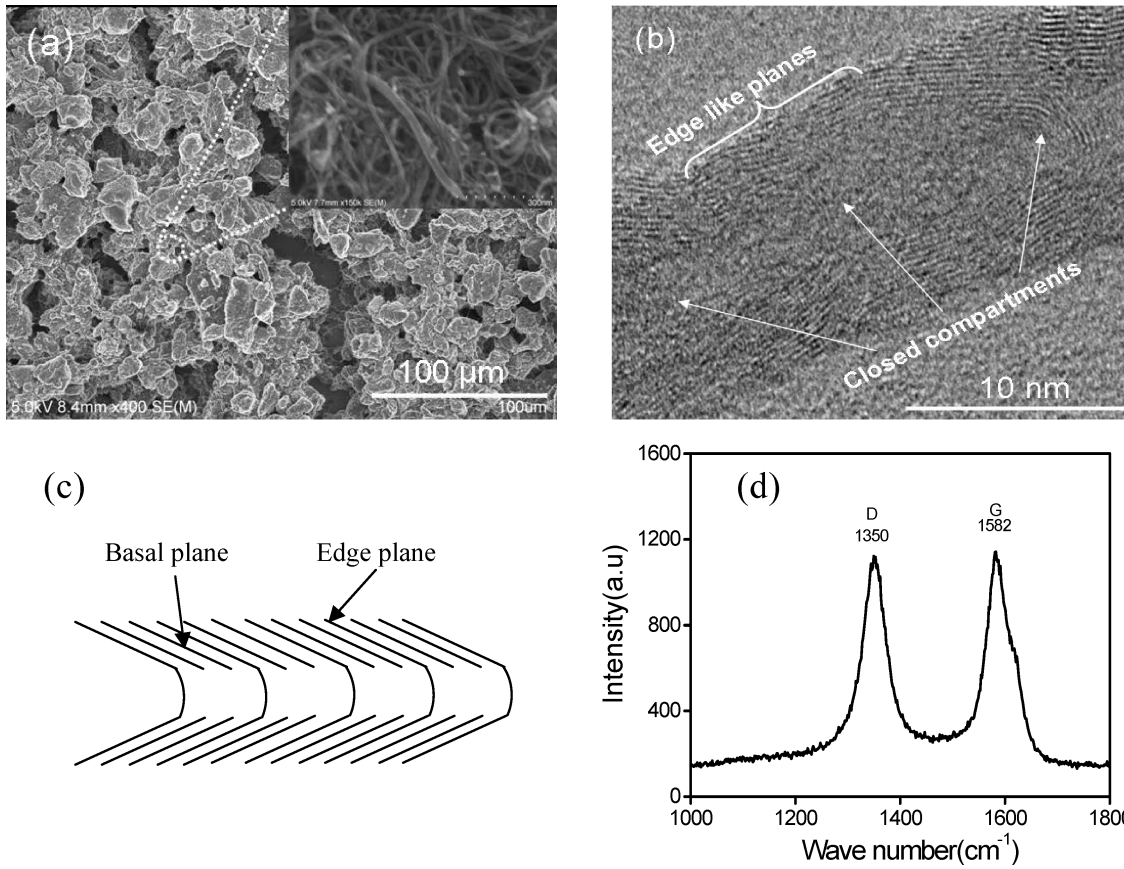

FIGURE 3. Microstructural characterization of multiwall CNTs: (a) FE-SEM image of a multiwall CNT/CMC composite film on a fluorine-doped SnO_2-conducting glass substrate. Inset: enlarged view of the marked portion. (b) TEM image of the bamboolike structure in multiwall CNTs used in this study. (c) Schematic of the bamboolike-structure multiwall CNT. (d) Raman spectrum of multiwall CNTs, using a 514-nm (argon-ion) wavelength laser probe.

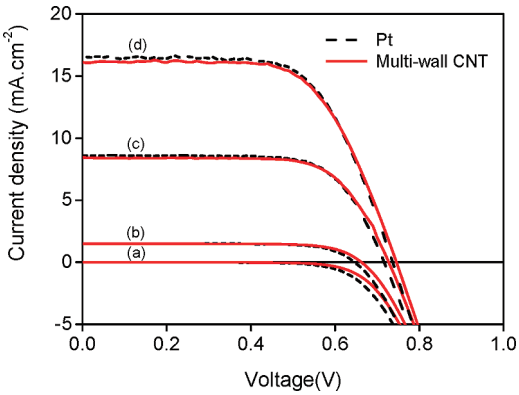

FIGURE 4. Current–voltage characteristics of DSSC with multiwall CNT (solid line) and platinum (dashed line) counter electrodes. Curve a shows the performance of devices in the dark. Curves b–d were measured under 0.1, 0.5, and 1 sun illumination (air mass 1.5 G), respectively.

light was calibrated by an NREL-certified silicon reference cell equipped with a KG-5 filter (16).

3. RESULTS AND DISCUSSION

The catalytic performance of CNT electrodes was evaluated by measuring the charge-transfer resistance (R_{CT}) in a thin-layer symmetric cell configuration. Figure 2 shows the Nyquist plots of multiwall CNT or platinum electrodes in a thin-layer symmetric cell configuration. The R_{CT} of a single electrode can be taken as half the value of the real component of impedance at a high-frequency side semicircle (4, 17). When the plots were fitted with the equivalent circuit (inset in Figure 2), R_{CT} of multiwall CNT electrode was found to be 0.82 $\Omega \cdot cm^2$. Under similar conditions, the screen-printed platinum electrode shows the corresponding value of 1.8 $\Omega \cdot cm^2$. The origin of such a high electrocatalytic property in multiwall CNT electrodes is still a subject of debate. For example, a few reports claimed that a large surface area and defect-rich edge planes can enhance the electron-transfer kinetics (18, 19), while other credited this to the residual catalyst particles (20). If the latter is the case, prolonged exposure of multiwall CNTs in a highly corrosive I^-/I_3^- electrolyte leads to the metal particles becoming dissolved; as a consequence, R_{CT} will increase. However, during the temporal evaluation, R_{CT} of the CNT electrode remains constant (see Figure S1 in the Supporting Information).

A low-magnification field-emission scanning electron microscopy (FE-SEM) image (Figure 3a) shows the formation of multiwall CNT aggregates with different size distribution on an FTO glass substrate. This was attributed to the high CNT concentration (10 wt %) and poor dispersion in the polymer-dissolved aqueous solution. The CNT aggregates mainly consist of a randomly oriented mesoporous nanotube network (see inset in Figure 3a). Because the dimensions of I_3^- ions in acetonitrile are only 3 Å in width and 6 Å in length, they can diffuse through the pores, be adsorbed onto the active site, and become reduced (21). As shown in Figure 3b, a transmission electron microscopy (TEM) image confirms the bamboolike structure of multiwall CNTs used in this study. The large number of transverse walls with periodically closed compartments results in edge planes at regular intervals along the tube surface. The high density of the defect-rich edge planes with an improved electrode–electrolyte interface might be responsible for the observed low R_{CT} in multiwall CNT electrodes (22). The Raman spectra (Figure 3d) further indicate the presence of defect-rich edge planes in bamboolike-structure multiwall CNTs. The disorder-

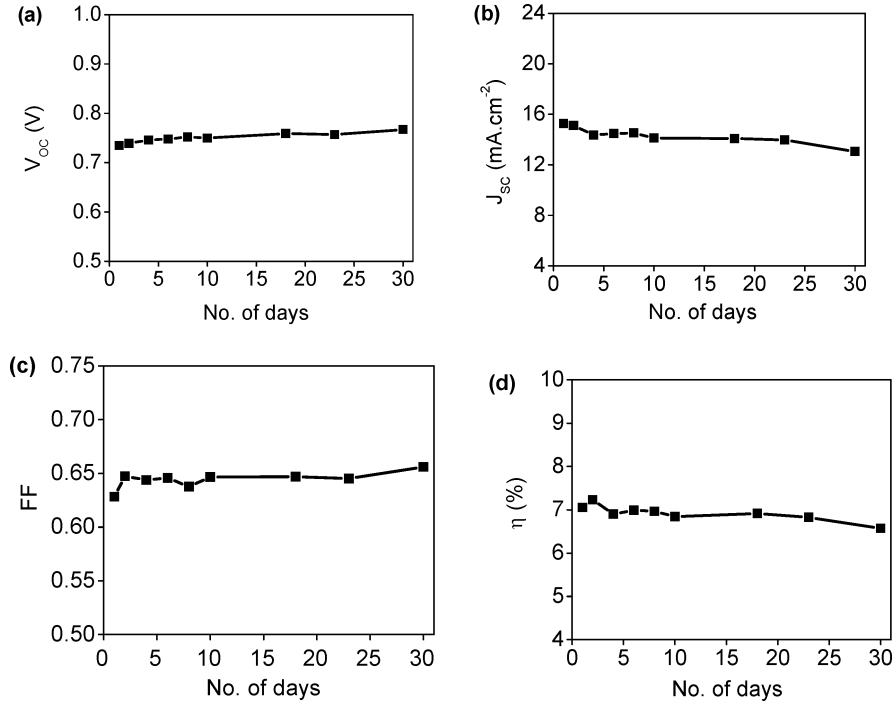

FIGURE 5. Variation if the current–voltage parameters of multiwall CNT counter-electrode DSSCs. The devices were aged in the dark at room temperature, and current–voltage measurements were carried out under 1 sun illumination (100 mW/cm^2, air mass 1.5 G) at regular intervals. (a) Open-circuit voltage, V_{OC}. (b) Short-circuit current density, J_{SC}. (c) Fill factor, FF. (d) Energy conversion efficiency, η.

Table 1. Current–Voltage Parameters of DSSC with Multiwall CNT and Platinum Counter Electrodes under Simulated Solar Illumination[a]

counter electrode	light intensity (mW/cm^2)	V_{OC} (V)	J_{SC} (mA/cm^2)	FF	η (%)
multiwall CNT	11	0.660	1.50	0.75	6.75
	54	0.720	8.41	0.71	7.96
	100	0.740	16.20	0.64	7.67
platinum	11	0.640	1.52	0.74	6.54
	54	0.710	8.60	0.71	8.03
	100	0.730	16.50	0.65	7.83

[a] All values are averages of three samples. The active area of the device was 0.36 cm^2.

induced D bands, which originated from defects or the finite size of the nanotubes, and the tangential G mode ascribed to the graphene structure were observed at 1350 and 1582 cm^{-1}, respectively. Because there are no distinguished carbon nanoparticles observed in the FE-SEM and TEM images, it is reasonable to attribute the higher intensity of the D band to defect-rich edge planes. The high value of the Raman ratio ($I_D/I_G = 0.9825$) also confirms the low graphitization degree of bamboolike-structure multiwall CNTs (23).

Figure 4 shows the current–voltage performance of multiwall CNT counter electrode DSSCs in the dark and at different levels of simulated solar illumination. Under 1 sun illumination (100 mW/cm^2, air mass 1.5 G), the open-circuit voltage (V_{OC}), short-circuit current density (J_{SC}), and fill factor (FF) of multiwall CNT counter-electrode DSSCs were 0.740 V, 16.2 mA/cm^2, and 0.64, respectively, yielding an energy conversion efficiency (η) of 7.67%. The corresponding values (V_{OC}, J_{SC}, FF, and η) of the platinum counter-electrode device were 0.730 V, 16.5 mA/cm^2, 0.65, and 7.83%, respectively. Despite the high V_{OC}, the multiwall CNT counter-electrode device shows a low η, owing to the small decrease in both J_{SC} and FF. The quasi-transparent platinum counter electrode, consisting of activated platinum nanoclusters on an FTO glass substrate, slightly reflects the unabsorbed portion of incident solar light toward the TiO_2 photoanode. However, this effect is completely obstructed in the opaque multiwall CNT counter electrode and hence has a relatively low J_{SC}. In addition, the mesoporous structure of the multiwall CNT film increased the diffusion impedance of redox species (represented by the low-frequency side of the semicircle in the Nyquist plot), which results in a large internal series resistance and low FF (24).

The major concern for the application of multiwall CNT counter electrodes in DSSC is long-term stability. During prolonged exposure in a corrosive electrolyte, weakly adhered multiwall CNTs may detach from the FTO glass substrate and get deposited on the TiO_2 photoanode side, promoting the dark current. Figure 5 shows the variation in the current–voltage parameters of sealed devices aged in the dark at room temperature. During the test, both V_{OC} and FF slightly increased as compared to fresh cells and then stabilized. In contrast, J_{SC} continuously decreased with time. The drop in J_{SC} was partially compensated for by enhancement of both V_{OC} and FF, and therefore the device almost maintains its initial day performance. The electrochemical impedance spectroscopy measurement, carried out under 1 sun illumination at open-circuit conditions, provides further insight into variation of the current–voltage parameters. The positive shift of the high-frequency peak reveals that the increase in FF arises from an accelerated electron-transfer process at a multiwall CNT counter electrode (see Figure S2 in the Supporting Information). Upon aging, the intermediate-frequency peak shifted to the low-frequency side, suggesting an increased electron lifetime in the TiO_2 conduction band. This observation is consistent with a decrease in the dark current (see Figure S3 in the Supporting Information) and explains the gradual increase in V_{OC} (25, 26).

4. CONCLUSIONS

In conclusion, we have shown that multiwall CNTs can be used as efficient electrocatalysts for triiodide reduction in DSSCs. A large number of defect-rich edge planes in bamboolike-structure multiwall CNTs ensure low charge-transfer resistance, and therefore the devices show FF and η values comparable to those of conventional platinum counter-electrode DSSCs. While these initial results are based on FTO glass substrates, we believe such a high performance can be reproduced in FTO-free CNT counter-electrodes for cost-effective volume production of DSSCs.

Acknowledgment. This work was supported by a grant from the Basic Science Research Program of the Korea Electrotechnology Research Institute.

Note Added after ASAP Publication. Reference 16 was modified in the version of this paper published ASAP May 15, 2009; the corrected version published ASAP June 3, 2009.

Supporting Information Available: Electrochemical impedance spectroscopy and dark current–voltage characteristics of fresh and aged CNT counter-electrode DSSCs. This material is available free of charge via the Internet at http://pubs.acs.org.

REFERENCES AND NOTES

(1) O'Regan, B.; Grätzel, M. *Nature* **1991**, *353*, 737–740.
(2) Grätzel, M. *Nature* **2001**, *414*, 338–344.
(3) Gregg, B. A. *J. Phys. Chem. B* **2003**, *107*, 4688–4698.
(4) Papageorgiou, N.; Maier, W. F.; Grätzel, M. *J. Electrochem. Soc.* **1997**, *144*, 876–884.
(5) Fang, X.; Ma, T.; Guan, G.; Akiyama, M.; Kida, T.; Abe, E. *J. Electroanal. Chem.* **2004**, *570*, 257–263.
(6) Olsen, E.; Hagen, G.; Lindquist, S. E. *Sol. Energy Mater. Sol. Cells* **2000**, *63*, 267–273.
(7) Papageorgiou, N. *Coord. Chem. Rev.* **2004**, *241*, 1421–1446.
(8) Kay, A.; Grätzel, M. *Sol. Energy Mater. Sol. Cells* **1996**, *44*, 99–117.
(9) Hino, T.; Ogawa, Y.; Kuramoto, N. *Carbon* **2006**, *44*, 880–887.
(10) Ramasamy, E.; Lee, W. J.; Lee, D. Y.; Song, J. S. *Appl. Phys. Lett.* **2007**, *90*, 173103.
(11) Murakami, T. N.; Ito, S.; Wang, Q.; Nazeerudin, M. K.; Bessho, T.; Cesar, I.; Liska, P.; Baker, R. H.; Comte, P.; Pechy, P.; Grätzel, M. *J. Electrochem. Soc.* **2007**, *153*, A2255–A2261.
(12) Huang, Z.; Liu, X.; Li, K.; Li, D.; Luo, Y.; Li, H.; Song, W.; Chen, L.; Meng, Q. *Electrochem. Commun.* **2007**, *9*, 596–598.
(13) Rakov, E. G. In *Nanotubes and Nanofibers*; Gogotsi, Y., Ed.; Taylor & Francis: New York, 2006; p 39.
(14) Suzuki, K.; Yamaguchi, M.; Kumagai, M.; Yanagida, S. *Chem. Lett.* **2003**, *32*, 28–29.

(15) Heng, L. Y.; Chou, A.; Yu, J.; Chen, Y.; Gooding, J. J. *Electrochem. Commun.* **2005**, *7*, 1457–1462.
(16) Lee, W. J.; Ramasamy, E.; Lee, D. Y. *Sol. Energy Mater. Sol. Cells* **2009**, *93*, 1448–1451.
(17) Hauch, A.; Georg, A. *Electrochim. Acta* **2001**, *46*, 3457–3466.
(18) Nugent, J. M.; Santhanam, K. S. V.; Rubio, A.; Ajayan, P. M. *Nano Lett.* **2001**, *1*, 87–91.
(19) Banks, C. E.; Davies, T. J.; Wildgoose, G. G.; Compton, R. G. *Chem. Commun.* **2005**, *7*, 829–841.
(20) Sljukic, B.; Banks, C. E.; Compton, R. G. *Nano Lett.* **2006**, *6*, 1556–1558.
(21) Sakane, H.; Mitsui, T.; Tanida, H.; Watanabe, I. *J. Synchrotron Radiat.* **2001**, *8*, 674–676.
(22) Shanmugam, S.; Gedanken, A. *Electrochem. Commun.* **2006**, *8*, 1099–1105.
(23) DiLeo, R. A.; Landi, B. J.; Raffaelle, R. P. *J. Appl. Phys.* **2007**, *101*, 064307.
(24) Han, L.; Koide, N.; Chiba, Y.; Islam, A.; Komiya, R.; Fuke, N.; Fukui, A.; Yamanaka, R. *Appl. Phys. Lett.* **2005**, *86*, 213501.
(25) Wang, Q.; Moser, J. E.; Grätzel, M. *J. Phys. Chem. B* **2005**, *109*, 14945–14953.
(26) Kuang, D.; Klein, C.; Ito, S.; Moser, J. E.; Baker, R. H.; Evans, N.; Duriaux, F.; Grätzel, C.; Zakeeruddin, S. M.; Grätzel, M. *Adv. Mater.* **2007**, *19*, 1133–1137.

AM800249K